ACS OMEGA

http://pubs.acs.org/journal/acsodf

Article

Synthesis and Characterization of the Nanogold-Bound Ternary Copper(II) Complex of Phenanthroline and Cysteine as Potential Anticancer Agents

Ahmad Junaid, Chew Hee Ng, and Ing Hong Ooi*

Cite This: *ACS Omega* 2022, 7, 26190−26200

Read Online

ACCESS | Metrics & More | Article Recommendations

ABSTRACT: The aim of this study was to synthesize and characterize a nanogold−$\{[(Cu)(phen)(cys)(H_2O)]NO_3\}_n$ conjugate and to evaluate its antiproliferative property against the breast cancer cell line (MCF7) and normal cell line (MCF10A). Nanogold solution was prepared using the Turkevich method. In one approach, a ternary copper(II) complex of 1,10-phenanthroline with L-cysteine, $[(Cu)(phen)(cys)(H_2O)]NO_3$, was first prepared and then tethered with the gold nanoparticles. In another approach, gold nanoparticles were reacted with L-cysteine, copper(II) nitrate, and 1,10-phenanthroline subsequently. The synthesized $[(Cu)(phen)(cys)(H_2O)]NO_3$ complex was characterized by Fourier transform infrared (FTIR) and electrospray ionization mass spectrometry techniques, which showed that L-cysteine was bound to the copper through carboxylic and amino groups, with the thiol moiety remaining free. The free thiol group was bound to the nanogold surface to form the nanogold−$\{[(Cu)(phen)(cys)(H_2O)]NO_3\}_n$ conjugate, as evidenced by the increase in the surface plasmon absorption band in ultraviolet−visible and the absence of a thiol peak in FTIR of the nanogold−copper complex conjugate. The anticancer activity of the nanogold−copper complex conjugate and the free copper complex against a breast cancer cell line (MCF7) and their toxicity on a normal cell line (MCF10A) were examined using the 3-(4,5-dimethylthiazol-2-yl)-5-(3-carboxymethoxy phenyl)-2-(4-sulfophenyl)-2*H*-tetrazolium assay. Results suggested that the nanogold−$\{[(Cu)(phen)(cys)(H_2O)]NO_3\}_n$ conjugate demonstrates a selective antiproliferative and proapoptotic effect on the breast cancer cells, confirming the potential of the nanogold−copper complex conjugate as an anticancer agent.

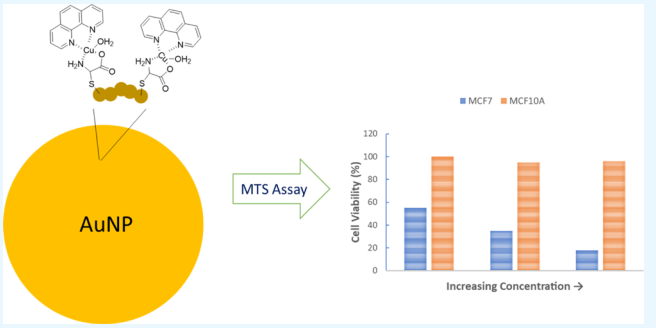

INTRODUCTION

As one of the three biologically active essential trace elements, copper plays a vital role in the wellbeing of humans and animals.[1−3] The overdose or lack of bodily copper can both cause serious failure in the modulation of life. For instance, copper deficiency[4] or copper toxicity due to overdose tends to cause higher reactive oxygen species production and, thus, oxidative damage to the cell, DNA, and proteins that could lead to various neurodegenerative diseases.[5]

Copper complexes, on the other hand, have been widely reported to be anticancer in vitro and in vivo, and some of them have moved on to clinical trials,[6] which adds another dimension to the field of biomedical applications.[7] Among other complexing ligands, 1,10-phenanthroline is used in conjugation with copper(II) ions to give copper(II) complexes that are anticancer.[8] The phenanthroline (Phen) was proven to be a contributing factor from copper(II) complexes in suppressing breast cancer cells.[9] The phenanthroline-based copper(II) complex showed cytotoxicity many times more than that of cisplatin.[10] Another example is $[Cu(Phen)LCl]\cdot 0.5H_2O$, which was reported to be cytotoxic against cultured human cancer cell lines.[11] Copper(II) complexes with two units of 1,10-phenanthroline also showed good anticancer properties.[12] On the other hand, the copper(II) L-cysteine complex was reported to be a black precipitate that was obtained from the oxidation of copper(I) cysteine.[13,14] Other studies on L-cysteine−copper complexes have been reported, whereby both carboxylate and amino groups[15] or just sulfhydryl groups[16] are utilized to form coordinate bonding with the copper ion center. Nonetheless, phenanthroline- and L-cysteine-based copper(II) complexes have never been reported. Nevertheless, it is envisaged that the sulfhydryl group of L-cysteine could be selectively bound to nanogold

Received: March 27, 2022
Accepted: May 12, 2022
Published: July 19, 2022

particle surfaces while the carboxylate and amino groups coordinate to copper(II) ions, which, thus, makes the nanogold−copper complex a potential metallodrug for anticancer therapy.

The gold nanoparticles of various forms, such as nanorods, nanocages, nanoshells, and nanostars, which possess strong absorbance and/or light scattering, have been extensively studied in cancer-specific bioimaging,[17] vaccine development,[18] anticancer drug delivery,[19] chemical and biological sensing,[20] and cervical cancer DNA purification.[21] Most gold nanoparticles, which are used for conjugation, are produced using the Turkevich method.[22] In general, gold nanoparticle conjugates could alter the pharmacokinetic properties of free drugs by increasing their solubility, stability, bio-distribution, permeation, and retention effects.[23,24] The negative charges on nanogold surfaces allow the conjugation of therapeutic drugs to happen easily, through which the cytotoxicity of some free anticancer drugs is enhanced, resulting in better cancer treatment efficacy.[25] As the thiol (−SH) functional group has strong affinity toward atomic gold surfaces, many gold conjugates have been prepared using this thiol−gold binding approach, such as gold−DNA as a contrast agent designed for the detection of the prostate-specific membrane antigen (PSMA),[26] gold−DNA conjugates for applications in nanotechnology and biotechnology,[27] gold−peptide for improving the radical scavenging properties and enhancing apoptosis in cancer cells,[28] and gold−antibody conjugates that enhance tissue repair.[29] In fact, gold nanoparticles have been shown to be nontoxic in many experiments.[30] Thus, the gold nanoparticle approach has emerged as an attractive strategy for targeted anticancer drug delivery. Nonetheless, collateral damage to normal cells is still a major problem that needs to be overcome or at least minimized to an acceptable level.[31,32]

Thus, we aim to synthesize and characterize a nanogold-conjugated copper complex having 1,10-phenanthroline and L-cysteine ligands and to examine its cytotoxicity against breast cancer cell lines (MCF-7) and normal cell lines (MCF-10A).

EXPERIMENTAL SECTION

Materials and Methods. Gold(III) chloride trihydrate (≥99.9%), intercalator ligand 1,10-phenanthroline (≥99%), L-cysteine (≥97%), and copper(II) nitrate trihydrate (98.0−103%) were purchased from Sigma-Aldrich (USA). Tri-sodium citrate dihydrate (99.95%) was purchased from Fisher Scientific. All the chemicals obtained were of analytical grade and were used as received. All the solutions for copper complex synthesis and gold nanoparticle synthesis were prepared using Milli-Q water.

Fourier transform infrared (FTIR) spectra were recorded as KBr pellets in the 4000−400 cm^{-1} range on a PerkinElmer spectrometer. The ultraviolet−visible (UV−vis) spectra of a sample dissolved in ultrapure water were recorded on a PerkinElmer Lambda 25 spectrophotometer in the 200−900 nm range. The electrospray ionization mass spectrometry (ESI-MS) spectra of the sample in water−methanol solutions were recorded from 50−1000 m/z on a PerkinElmer benchtop quadrupole ion trap mass spectrometer (Flexar SQ300) with the capillary temperature set to 60 °C.

Synthesis of Copper Complex [Cu(phen)(cys)(H_2O)]NO_3. [Cu(phen)(cys)(H_2O)]NO_3 was synthesized according to a reported procedure with modification.[33] The molar ratio of copper nitrate, 1,10-phenanthroline, and L-cysteine was 1:1:1. A 5 mL ethanol solution of 1,10-phenanthroline (0.005 M; pH 8.07) was added to a 5 mL aqueous solution of $Cu(NO_3)_2{\cdot}3H_2O$ (0.005 M) dropwise. The resultant Cu(phen)$(NO_3)_2$ solution was clear dark blue with a pH of 2.87. A 10 mL of L-cysteine aqueous solution (0.0025 M; pH 5.02) was added into the Cu(phen)$(NO_3)_2$ solution with mild heating to yield a dark green cloudy solution with a pH of 0.76. The cloudy solution obtained was then filtered using vacuum suction and a dark blue clear filtrate was obtained. A sodium bicarbonate solution (0.5 M) was added dropwise until the pH of the filtrate was raised from 0.76 to 4.81. The blue precipitate formed was collected by filtration and then dried in an oven at 60 °C for 2 h. The percentage yield of the copper complex was 67%. The dried precipitate was then characterized using FTIR, UV−vis, and MS.

Synthesis of Gold Nanoparticles. All the glassware used for this synthesis was washed with aqua regia (HNO_3/3HCl) and dried overnight prior to use. Gold nanoparticles were synthesized using the Turkevich method.[34] In this method, tri-sodium citrate was used to reduce and to stabilize the gold nanoparticles.[35]

Briefly, a 200 mL of chloroauric acid solution (1×10^{-4} M) was heated under reflux. A 4 mL aliquot of 0.5% (wt/wt) tri-sodium citrate was added through the condenser. The color of the solution was pale yellow. The mixture was heated vigorously for 30 min with stirring. During the reduction, the color of the solution changed from pale yellowish to ruby red. The resulting ruby red solution was cooled to room temperature with constant stirring. The UV−vis spectrometer and Zetasizer were then used to confirm the formation of gold nanoparticles and their size distribution and zeta potential, respectively.

Preparation of the Gold Copper Complex {[Cu(phen)(cys)(H_2O)]NO_3} Conjugate. Two methods were used for the functionalization of gold nanoparticles with the copper complex. The first method was the step-by-step addition of L-cysteine, copper nitrate, and 1,10-phenanthroline into the nanogold solution. The second method was by the addition of a pre-formed copper(II) complex into the nanogold solution.

(a) Three-Step Addition Method. The L-cysteine solution in water (1×10^{-4} M) was added into the gold nanoparticles solution in a volume ratio of 5:1. The resulting solution was stirred for 12 h at room temperature, which gradually changed from red to blue. The blue solution was dialyzed in a Spectra/Por 7 pretreated regenerated cellulose (RC; MWCO:1.0 kDa) membrane against ultrapure water for 6 h with water changed at every 30 min to remove any unbound L-cysteine molecules.

A copper nitrate aqueous solution (1×10^{-4} M) was added into the same solution in a 5:1 volume ratio and stirred for 30 min with mild heating at 40 °C to facilitate the binding of copper to L-cysteine. The mixture was then dialyzed for 3 h in the RC membrane (MWCO:1.0 kDa) to remove any unbound copper nitrate molecules.

Similarly, the 1,10-phenanthroline solution in ethanol (1×10^{-4} M) was mixed with the nanogold solution (1×10^{-4} M) in a volume ratio of 5:1, and allowed to react for 30 min, followed by 3 h of dialysis in the RC membrane (MWCO:1.0 kDa) to remove any unreacted molecules. The solution was clear with minute blue particles dispersed inside. The final solution was then characterized using UV−vis spectroscopy, and the dried sample was analyzed by FTIR spectroscopy.

(b) One-Step Addition Method. An aqueous solution of [Cu(phen)(cys)(H_2O)]NO_3 (1×10^{-4} M) was added to the nanogold solution (1×10^{-4} M) in a volume ratio of 5:1 and

https://doi.org/10.1021/acsomega.2c01858
ACS Omega 2022, 7, 26190−26200

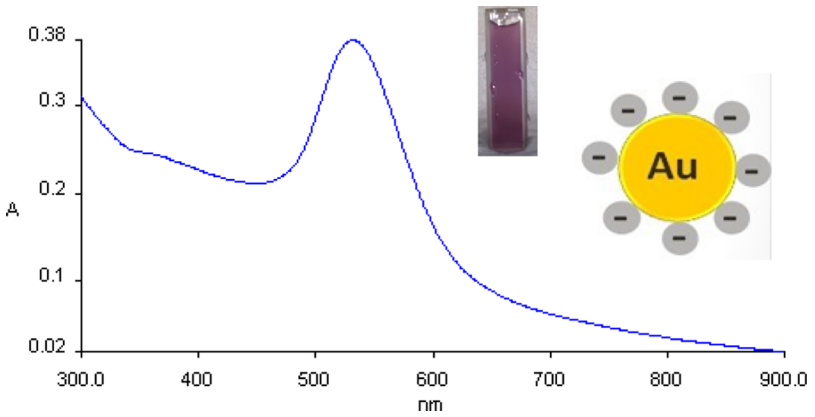

Figure 1. UV−vis spectrum of the nanogold solution.

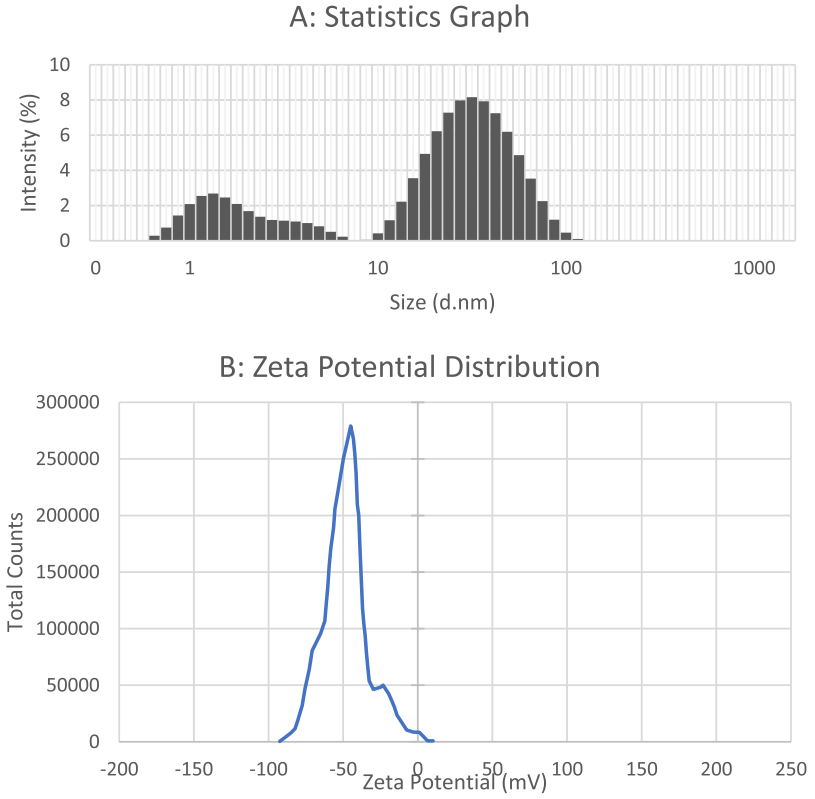

Figure 2. Average size of gold nanoparticles (A) and zeta potential of gold nanoparticles (B).

stirred for 12 h, followed by dialysis against deionized water for 6 h using a Spectra Por 7 RC membrane (MWCO: 1.0 kDa) to remove any unconjugated copper complex. The resulting solution was then analyzed by UV−vis spectroscopy, and the dried solid of the conjugate was analyzed by FTIR spectroscopy.

MTS Assay. The cell viability of MCF7 (the breast cancer cell line) and MCF10A (the normal cell line) was determined using a 3-(4,5-dimethylthiazol-2-yl)-5-(3-carboxymethoxy phenyl)-2-(4-sulfophenyl)-2*H*-tetrazolium (MTS) assay. MCF7 cells and MCF10A cells were seeded at a density of 30,000 cells in 63 μL of medium per well and 15000 cells in 63 μL medium per well, respectively. The cells were counted using a cell counting chamber slide (Invitrogen, C10283). The cells were then incubated at 37 °C in a 5% CO_2 incubator for 48 h.

The test compound $[Cu(phen)(cys)(H_2O)]NO_3$-functionalized gold nanoparticles (samples A and B) and $[Cu(phen)(cys)(H_2O)]NO_3$, all at 10-fold dilution, were added into the 96-well plate and incubated under the same conditions for 48 h. All the samples were filtered before use with a 0.22 μm syringe filter to remove any possible bacteria.

After 48 h of incubation, the cells were treated with 14 μL of the MTS solution (in each well) and incubated for 4 h under the same condition. The incubated plates were then read using an EnVision 2014 Multiple Label Reader at a wavelength of 490 nm with background subtraction at 630 nm. Optical density was determined using the following formula:

The cell viability of the cell line by the treated samples of various concentrations and cisplatin (positive control) was determined in reference to the untreated control (negative

https://doi.org/10.1021/acsomega.2c01858
ACS Omega 2022, 7, 26190−26200

control). All the experiments were performed in triplicate and repeated three times. Cell viability was calculated from

$$[(\mathrm{Ti} - \mathrm{Tz})/(C - \mathrm{Tz})] \times 100$$

for concentrations for which Ti ≥ Tz

$$[(\mathrm{Ti} - \mathrm{Tz})/\mathrm{Tz}] \times 100$$

for concentrations for which Ti < Tz

whereby (average OD of each untreated cell lines) − (average OD of blank) = Tz; (average OD of each treated cells) − (average OD of blank) = Ti; OD = optical density; GI_{50} = concentration for 50% of maximal inhibition of cell proliferation; TGI = concentration of the compound which inhibits 100% of cell growth, (Ti = Tz); LD_{50} = dose that kills 50% of the treated cells; Tz = optical density of cells before treatment; Ti = optical density of cells after treatment; C = OD of control cells; and blank = medium only.

RESULTS AND DISCUSSION

Synthesis of Gold Nanoparticles. Figure 1 shows the UV−vis spectrum of a nanogold solution prepared by the Turkevich method. The plasmon resonance absorption peak maximum around λ_{max} 529 nm showed evidence of gold nanoparticle formation.[34,36] The ruby red color of the solution also confirmed the formation of the gold nanoparticles and this is consistent with the reported work.[34,37]

The thermodynamic size distribution and the zeta potential were analyzed using Zetasizer at 25 °C ± 0.1 °C. Figure 2 shows the results of the size distribution and zeta potential of the gold nanoparticles. The sizes of the nanoparticles ranged from 1 to 100 nm, with an average size of 14.38 nm, while the zeta potential of the prepared gold nanoparticles was −49.3 mV. This high zeta potential of the gold hydrosol also confirmed the formation of negatively charged citrate-stabilized gold nanoparticles.[34]

Synthesis of the [Cu(phen)(cys)(H_2O)]NO_3 Complex. [Cu(phen)(cys)(H_2O)]NO_3 (Figure 3) was prepared using a reported method with modification.[37] It was reported that similar compounds $[Cu(phen)(aa)H_2O]^+NO_3^-$ (aa: glycine; DL-alanine; L-threonine) had a distorted square pyramidal geometry.[38,39] In our study, the complex obtained was a blue precipitate, and an attempt to recrystallize the complex was unsuccessful. Thus, elemental analysis was not performed.

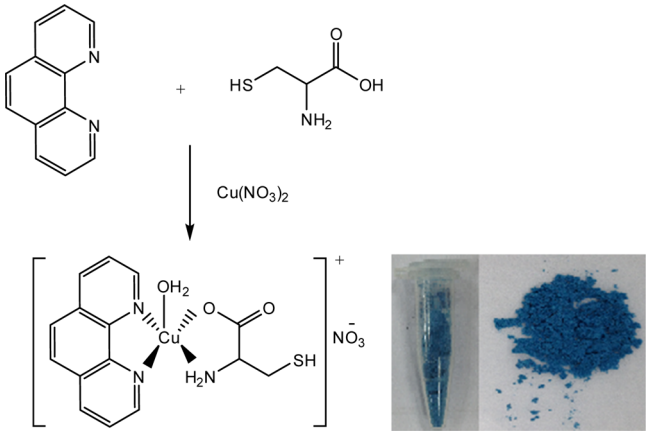

Figure 3. Synthesis scheme of the [Cu(phen)(cys)(H_2O)]NO_3 complex.

However, FTIR and ESI-MS were used to verify the proposed structure.

FTIR Analysis of the [Cu(phen)(cys)(H_2O)]NO_3 Complex. Figure 4 and Table 1 show the FTIR spectra and IR peak assignments of the complex, respectively. The broad IR band around 3200 cm^{-1} and the sharp band at 1519 cm^{-1} were attributed to the NH stretching and bending vibrations of chelated L-cysteine. In addition, two medium width bands at 1637 and 1431 cm^{-1} were due to the asymmetric and symmetric carboxylic group (COO−) stretching vibration of chelated L-cysteine. The free thiol (−SH) stretching vibration occurred at 2632 cm^{-1}. This indicated that cysteine was bound to the copper surface via its carboxylic group (COO−) and amino ($-NH_2$) groups. The broad band at 3412 cm^{-1} was due to the stretching vibration of the hyrdroxyl (−OH) group of coordinated water molecules, a Lewis base that contributes to the formation of the stable copper ion complex structure. Two sharp and strong peaks around 723 and 852 cm^{-1} are characteristic peaks of metal-chelated 1,10-phenanthroline.[40,41] A sharp peak at 1107 cm^{-1} was characteristic of the nitrate ion (NO_3^-). Thus, the[Cu(phen)(cys)(H_2O)]NO_3 complex structure is confirmed.

ESI-MS Studies of the [Cu(phen)(cys)(H_2O)]NO_3 Complex. According to the proposed copper complex structure, [Cu(phen)(cys)(H_2O)]NO_3, its molecular mass would be 444 Da. In the positive ion mode, the ESI-MS would detect only the positive ion and, thus, the nitrate ion would not be detected. Moreover, the apical water molecule of the complex, which is loosely bound, could be easily lost under the ionization conditions of ESI-MS. The loss of water molecules, under ionization conditions, was also reported in similar type of copper(II) complexes with phenanthroline and methylated glycine.[38] Hence, the expected molecular mass in ESI-MS of the copper complex after the omission of the nitrate ion and water molecule would be 363.89 Da.

An ESI-MS spectrum of the copper complex in MS grade methanol is shown in Figure 5. The presence of the intense peaks at m/z 363.49 corresponded to the ion fragment Cu(phen)(cys) that further confirmed the proposed copper complex structure.

This also showed that there is no dissociation of phenanthroline and the amino acid cysteine under the MS operating conditions.

UV−vis Spectrum of the [Cu(phen)(cys)(H_2O)]NO_3 Complex. Figure 6 shows the UV−vis spectrum of the copper complex measured in Milli-Q water. The absorbance peak at 613 nm is a typical d−d transition band of copper(II) complexes in the aqueous solution.[40]

Conjugation of the [Cu(phen)(cys)(H_2O)]NO_3 Complex to Gold Nanoparticles. The gold nanoparticles were linked to the [Cu(phen)(cys)(H_2O)]NO_3 complex by two methods.

Three-Step Addition Method. In this method, L-cysteine, copper, and phenanthroline were added step-by-step into the same nanogold solution. Each step was immediately followed by a dialysis with an RC dialysis membrane (MWCO 1 kDa) to remove any vestigial molecules before the UV−vis spectrum was recorded. It was observed that with the addition of cysteine, another plasmon band appeared at around λ_{max} = 740 nm, as shown in Figure 7. This bathochromic shift suggests the aggregation due to the ionic interaction between the pair of negatively charged carboxylate and positively charged amino

https://doi.org/10.1021/acsomega.2c01858
ACS Omega 2022, 7, 26190−26200

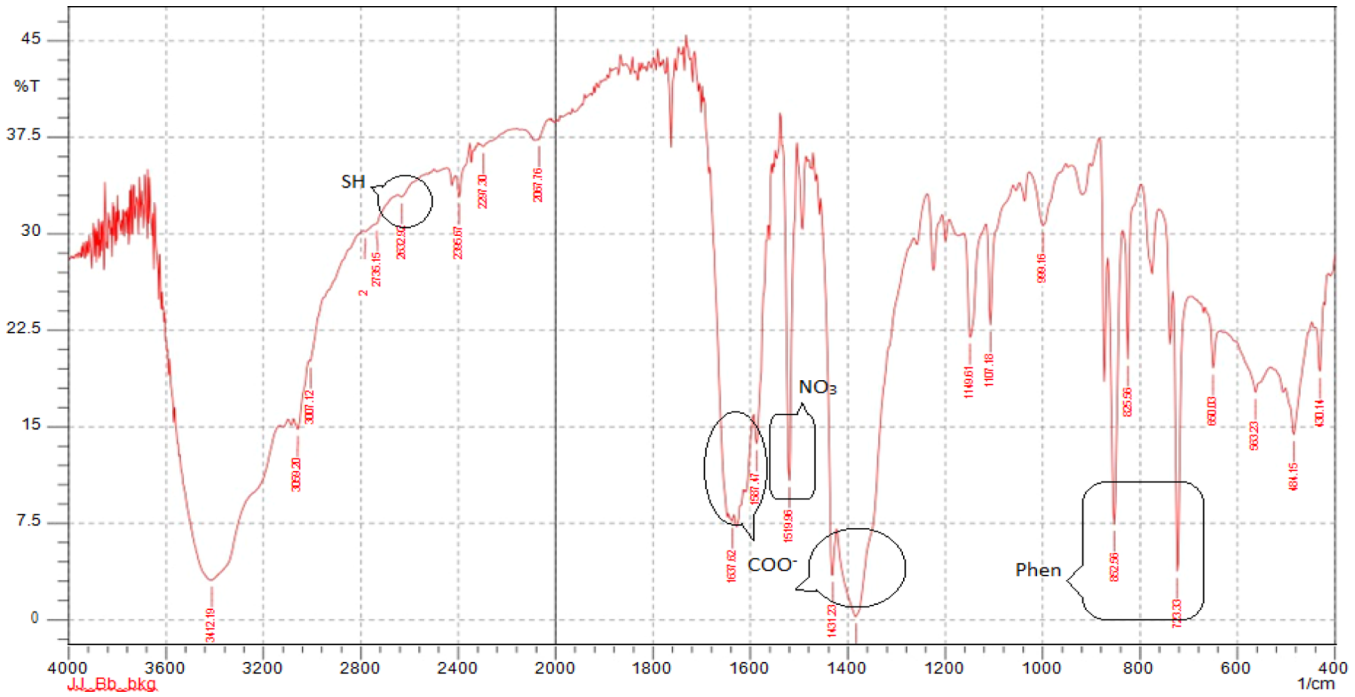

Figure 4. FTIR spectrum of the $[Cu(phen)(cys)(H_2O)]NO_3$ complex.

Table 1. FTIR Peak Assignment of Nanogold–$\{[Cu(phen)(cys)(H_2O)]NO_3\}_n$ Conjugates and Their Comparison with Those of the Free $[Cu(phen)(cys)(H_2O)]NO_3$ Complex

functional group	major FTIR bands of $[Cu(phen)(cys)(H_2O)]NO_3$	major FTIR bands of the nanogold complex of $[Cu(phen)(cys)(H_2O)]NO_3$
copper(II)-chelated 1,10-phenanthroline characteristics peaks	723.33 cm^{-1}, 852.56 cm^{-1}	721.4 cm^{-1}, 852.56 cm^{-1}
COO−	1431.23 cm^{-1}, 1637.62 cm^{-1}	1425.44 & cm^{-1}, 1624.12 cm^{-1}
−SH	2632.92 cm^{-1}	absent

functional groups of two cysteine molecules, which were bound to gold nanoparticles via thiol functional groups.[37]

Another observation was the rapid color change of the nanogold solution from ruby red to blue after the addition of the cysteine solution, indicating the reaction between the nanogold solution and cysteine (Figure 8). This phenomenon can be easily understood; when light is shone on the surface of a metal, it causes the metal electrons to vibrate. When the frequency of the movement of metal electrons matches that of the incident light frequency, resonance occurs. As a result, the portion of the light with that frequency will be absorbed and the rest scattered, producing the corresponding color. The electrons of gold nanoparticles resonate at a frequency within the visible range of light. Small-sized particles look red because they resonate and absorb green, purple, yellow, and blue wavelengths of light. Similarly, larger particles resonate and absorb yellow, green, and red wavelengths of visible light, so

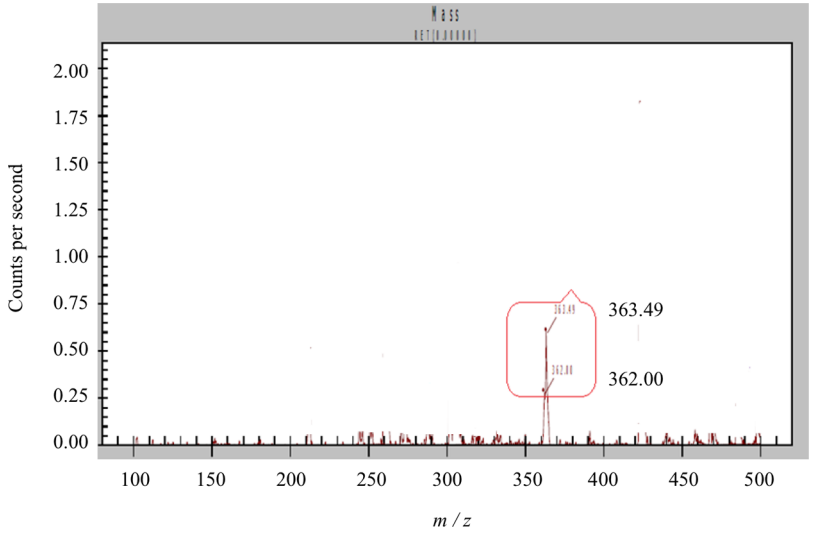

Figure 5. ESI-MS spectrum of the $[Cu(phen)(cys)]$ ion fragment.

https://doi.org/10.1021/acsomega.2c01858
ACS Omega 2022, 7, 26190−26200

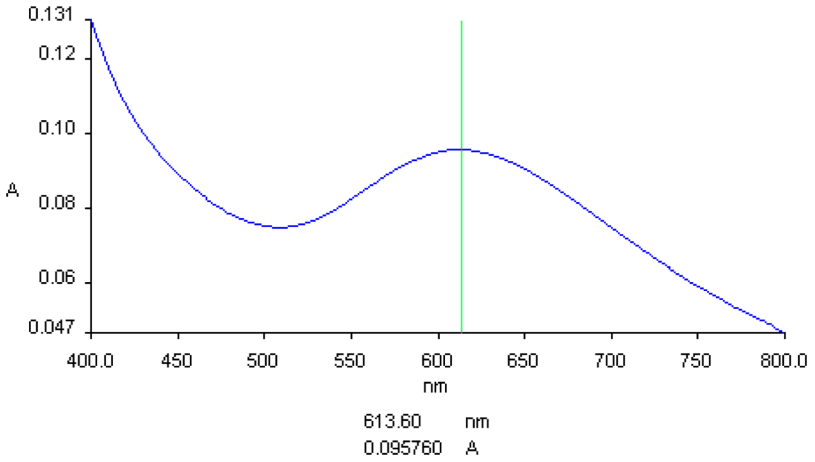

Figure 6. UV−vis spectrum of the $[Cu(phen)(cys)(H_2O)]NO_3$ complex.

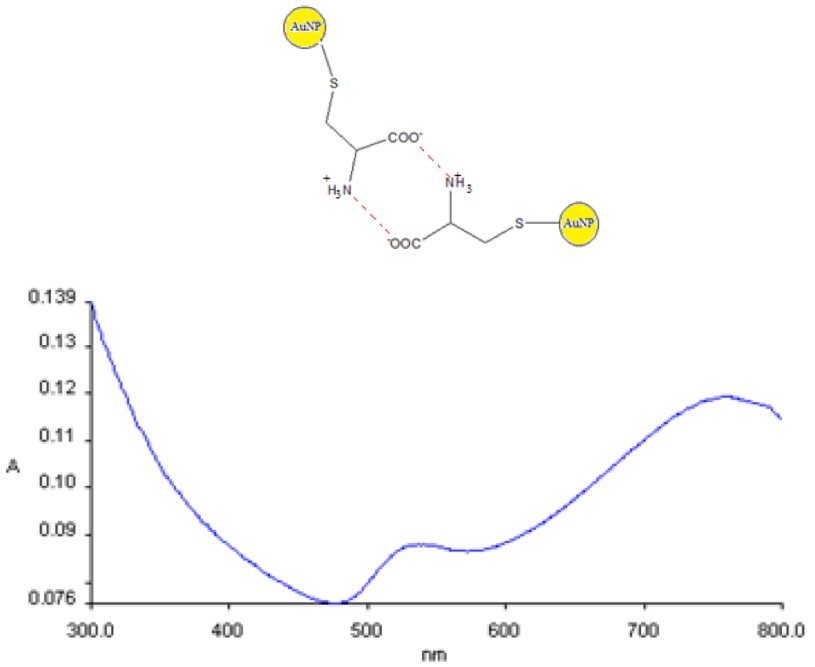

Figure 7. UV−vis spectrum of gold nanoparticles functionalized with cysteine.

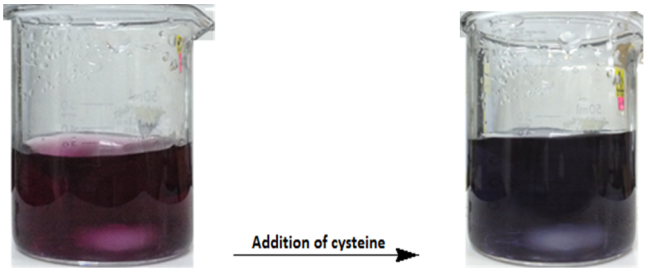

Figure 8. Color change observed when cysteine was added to the nanogold solution.

they look blue.[37] Hence, the increase in the size of gold nanoparticles causes the change in color from red to blue.

The addition of copper nitrate to the cysteine−nanogold conjugate was completed by a brief heating. This is because copper metal requires heat to overcome the electrostatic interaction between the cysteine-functionalized gold nanoparticles. Upon the addition of phenanthroline, the solution became clear with tiny blue particles suspended in it. The UV−vis spectrum of the resulting product in ultrapure water is shown in Figure 9. The very broad peak at a longer wavelength suggests the formation of desired nanogold−$[Cu(phen)(cys)(H_2O)]_n$ conjugates.

One-Step Addition Method. In this method, a solution of the $[Cu(phen)(cys)(H_2O)]NO_3$ complex (1×10^{-4} M) and the nanogold solution (1×10^{-4} M) in a volume ratio of 5:1 were mixed and reacted followed by dialysis. The color of the nanogold solution changed from ruby red to blue upon the addition of the copper complex. After 12 h of reaction, the color of the solution changed from blue to colorless with a blue precipitate suspended in the solution. Figure 10 shows the UV−vis spectrum of the final solution. Similar broadening of the peak at a longer wavelength around $\lambda_{max} \sim 800$ nm as that of the three-step addition method was observed, which confirmed the formation of $[Cu(phen)(cys)(H_2O)]NO_3$-functionalized gold nanoparticles. This result shows that the

https://doi.org/10.1021/acsomega.2c01858
ACS Omega 2022, 7, 26190−26200

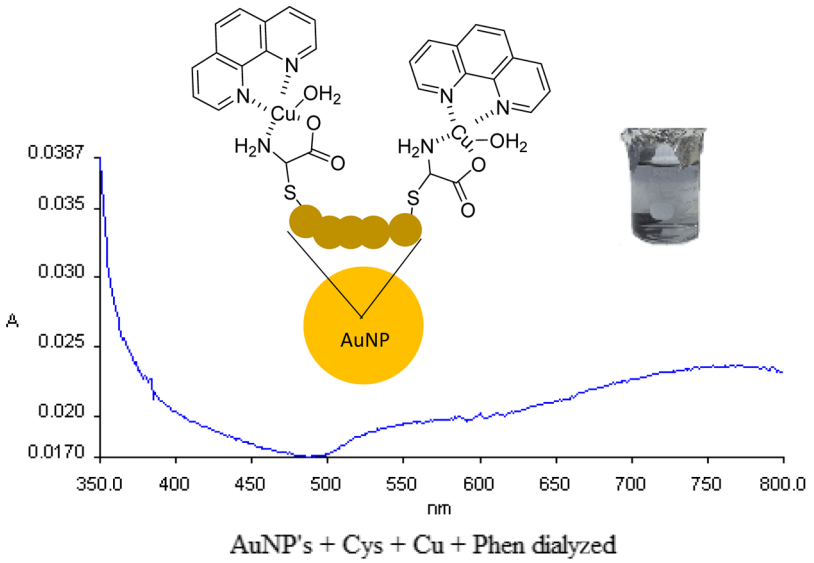

Figure 9. UV−vis spectrum of $[Cu(phen)(cys)(H_2O)]NO_3$-functionalized gold nanoparticles by the three-step addition method.

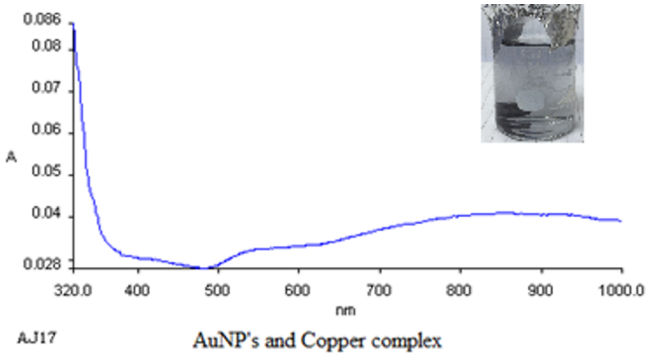

Figure 10. UV−vis spectrum of $[Cu(phen)(cys)(H_2O)]NO_3$-functionalized gold nanoparticles by the one-step addition method.

two methods have produced the same nanogold−$[Cu(phen)(cys)(H_2O)]_n$ conjugate.

FTIR Analysis of the $[Cu(phen)(cys)(H_2O)]NO_3$-Functionalized Gold Nanoparticles. As the nanogold−$\{[Cu(phen)(cys)(H_2O)]NO_3\}_n$ conjugate was prepared in water as a reaction medium, drying was done in vacuum concentrator at 45 °C for 24 h. The solid conjugates thus obtained were then kept in an oven at 50 °C overnight for further drying. The dried solid was then analyzed by FTIR using KBr pellets. The FTIR spectrum of nanogold−$\{[Cu(phen)(cys)(H_2O)]NO_3\}_n$ conjugate is shown in Figure 11. Table 1 compares the major IR bands of the nanogold−$\{[Cu(phen)(cys)(H_2O)]NO_3\}_n$ conjugates and those of the free $[Cu(phen)(cys)(H_2O)]$ complex.

The characteristic peaks of phenanthroline at 721 and 852 cm^{-1} and of the carboxylate ion ($-COO^-$) at 1425 cm^{-1} (symmetrical bending), 1624 cm^{-1} (asymmetrical bending), and amine (N−H) at around 3400 cm^{-1} of cysteine confirmed the coordination of phenanthroline and cysteine to copper in the nanogold−$\{[Cu(phen)(cys)(H_2O)]NO_3\}_n$ conjugates. The bathochromic shifts of phenanthroline representative peaks (from 723 to 721 cm^{-1}) and of the carboxylate ion (COO−) peaks (from 1431 and 1637 cm^{-1} to 1425 and 1624 cm^{-1}, respectively) were due to a change in the dipole moment of the nanogold complex. The S−H vibration band at 2632 cm^{-1}, which is present in the FTIR spectrum of $[Cu(phen)(cys)(H_2O)]NO_3$, was not observed in the FTIR spectrum of the nanogold−$\{[Cu(phen)(cys)(H_2O)]NO_3\}_n$ conjugate. Hence, the copper complex was bonded to the gold nanoparticles via the sulfur atom of cysteine.

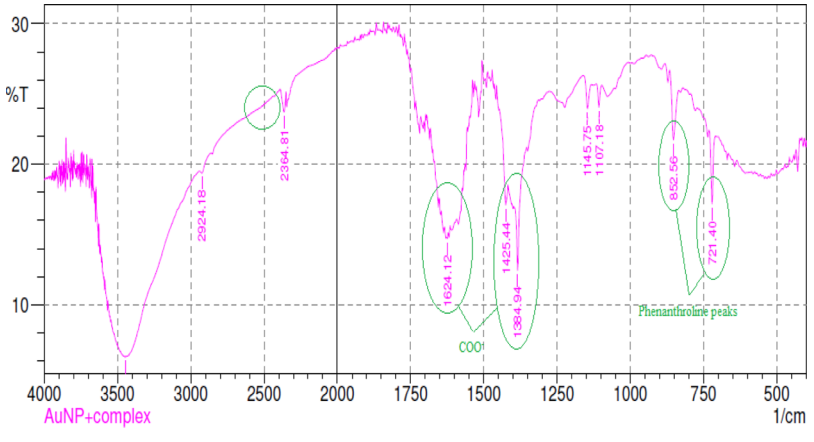

Figure 11. FTIR spectrum of the nanogold−$\{[Cu(phen)(cys)(H_2O)]NO_3\}_n$ conjugate.

https://doi.org/10.1021/acsomega.2c01858
ACS Omega 2022, 7, 26190−26200

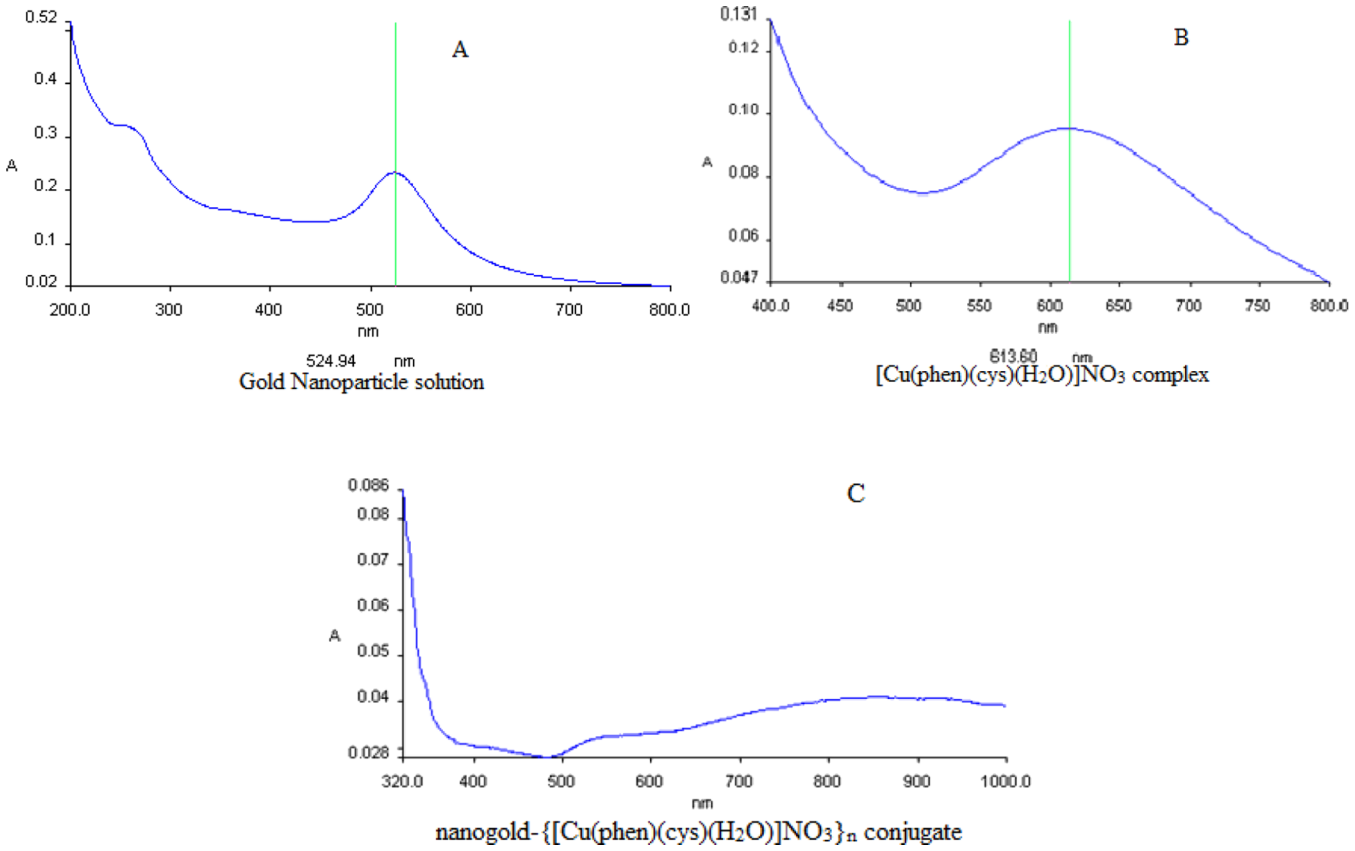

Figure 12. Comparison of UV−vis spectra of the (A) gold nanoparticle solution (0.0001 M), (B) $[Cu(phen)(cys)(H_2O)]NO_3$ complex (0.0001 M), and (C) nanogold−$\{[Cu(phen)(cys)(H_2O)]NO_3\}_n$ conjugate (0.0001 M) in ultrapure water.

Figure 12 shows the UV−vis spectra of the gold nanoparticles, $[Cu(phen)(cys)(H_2O)]NO_3$ and nanogold−$\{[Cu(phen)(cys)(H_2O)]NO_3\}_n$ conjugates in ultrapure water. The spectrum of nanogold−$\{[Cu(phen)(cys)(H_2O)]NO_3\}_n$ conjugates showed the broadening of the absorption band at a longer wavelength $\sim\lambda_{max}$ = 850 nm, which suggested the formation of the nanogold−$[Cu(phen)(cys)(H_2O)]_n$ conjugates.

Sizes of Nanogold−$\{[Cu(phen)(cys)(H_2O)]NO_3\}_n$ Conjugates Using Zetasizer. Zetasizer was used to measure particle size. The size of the as prepared nanogold−$\{[Cu(phen)(cys)(H_2O)]NO_3\}_n$ conjugates was in the range of 200−2500 nm. Because the conjugate with a smaller size is of interest to our study, syringe filters of 0.22 and 0.45 μm were used to filter out the larger aggregated product. Figure 13 shows the UV−vis spectra of the corresponding nanogold−$\{[Cu(phen)(cys)(H_2O)]NO_3\}_n$ conjugates and the $[Cu(phen)(cys)(H_2O)]NO_3$ complex solution, respectively. The bathochromic shifting of the UV−vis band of nanogold−$\{[Cu(phen)(cys)(H_2O)]NO_3\}_n$ conjugates (λ_{max} = 675 nm) with respect to that of the $[Cu(phen)(cys)(H_2O)]NO_3$ complex (λ_{max} = 622 nm) becomes smaller. Both filters were equally effective in removing larger aggregated products. For anticancer studies, all the samples were filtered with a 0.22 μm syringe filter prior to the test.

Anticancer Studies. The antiproliferative property of the nanogold−$\{[Cu(phen)(cys)(H_2O)]NO_3\}_n$ conjugate was examined using the MTS assay. The conjugates were incubated with breast cancer cell lines (MCF7) and non-cancer cell lines (MCF10A), respectively, in 96-well plates for 2 days. The absorbance was then read using a multiple label reader at a wavelength of 490 nm. The negative control in this experiment was the control well in which no drug or nanoparticles were added, while cisplatin was used as the positive control. Figures 14 and 15 show the results of the MTS assay of MCF10A and MCF7 cell viability, respectively.

In the cell viability−concentration curves, the red, blue, and green lines represented the copper complex $\{[Cu(phen)(cys)(H_2O)]NO_3\}$, sample A (nanogold−$\{[Cu(phen)(cys)(H_2O)]NO_3\}_n$ conjugates prepared by the one-step addition method), and sample B (nanogold−$\{[Cu(phen)(cys)(H_2O)]NO_3\}_n$ conjugates prepared by the three-step addition method). These samples with a 10-fold serial dilution were evaluated. The initial undiluted concentration of the nanogold complex test sample was assumed to be the same as the nanogold solution concentration at the preparation stage.

The nanogold−$\{[Cu(phen)(cys)(H_2O)]NO_3\}_n$ conjugates showed no effect on the normal cell line (MCF10A) in the tested micromolar range, while the same conjugates caused an inhibition and killing of the breast cancer cell line (MCF7). The GI_{50}, TGI, and LD_{50} values of the nanogold−$\{[Cu(phen)(cys)(H_2O)]NO_3\}_n$ conjugates and the $[Cu(phen)(cys)(H_2O)]NO_3$ complex on MCF10A and MCF7 are computed and summarized in Tables 2 and 3, respectively.

The ratio of LD_{50} values of nanogold−$\{[Cu(phen)(cys)(H_2O)]NO_3\}_n$ conjugate in MCF10A to MCF7 would show the distinct antiproliferative selectivity of conjugates toward the cancer cells than normal cells. The sample A and sample B showed the death of breast cancer cells at 8.3 and 8.1 μM, respectively.

https://doi.org/10.1021/acsomega.2c01858
ACS Omega 2022, 7, 26190−26200

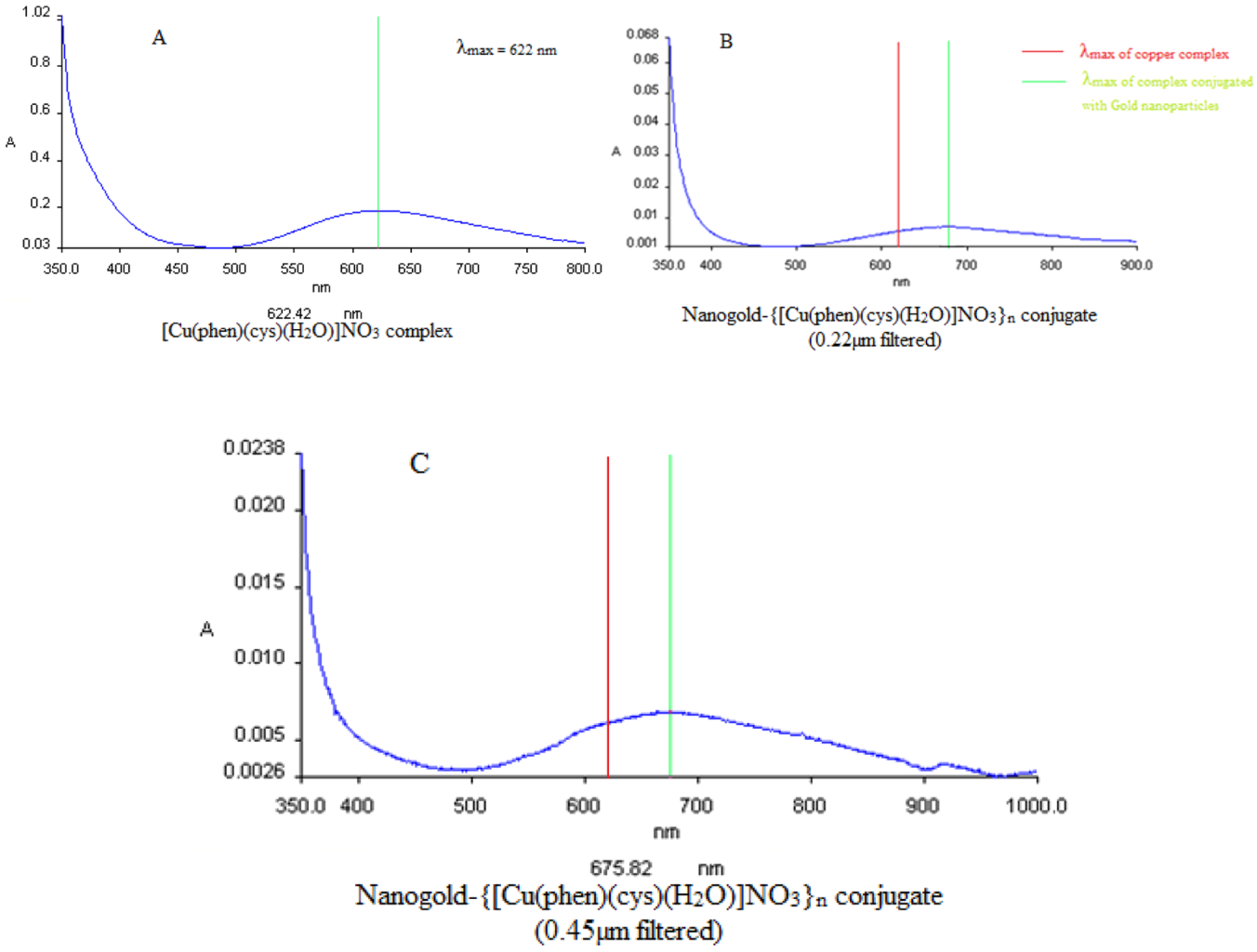

Figure 13. UV−vis spectra of the (A) $[Cu(phen)(cys)(H_2O)]NO_3$ complex, (B) nanogold−$\{[Cu(phen)(cys)(H_2O)]NO_3\}_n$ conjugates (0.22 μm filtered), and (C) nanogold−$\{[Cu(phen)(cys)(H_2O)]NO_3\}_n$ conjugates (0.45 μm filtered).

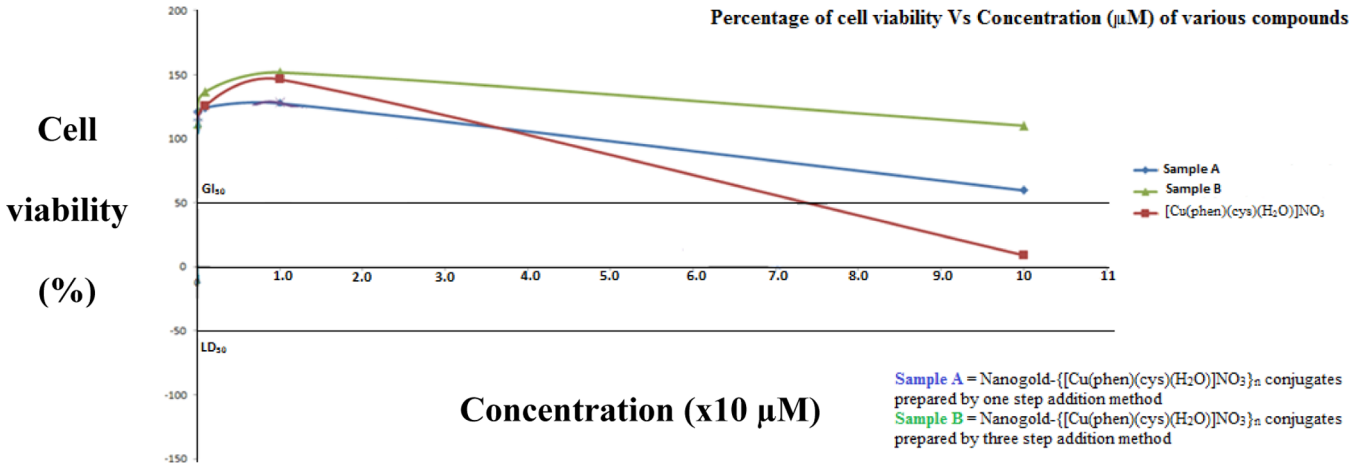

Figure 14. MTS assay of nanogold−$\{[Cu(phen)(cys)(H_2O)]NO_3\}_n$ conjugates on a normal cell line (MCF10A).

The free $Cu(phen)(cys)(H_2O)]NO_3$ complex also did not show any killing of the normal cell in the tested concentration range. However, it caused the inhibition of the normal cells at 7.2 μM. On breast cancer cell lines, the free $[Cu(phen)(cys)(H_2O)]NO_3$ complex caused the death of the cancer cells in the tested concentration range. These results showed that conjugating the $[Cu(phen)(cys)(H_2O)]NO_3$ complex with gold nanoparticles had made the complex more selective toward the cancerous cells than the normal cells and, at the same time, caused no effect on the normal cell.

The "n" in nanogold−$\{[Cu(phen)(cys)(H_2O)]NO_3\}_n$ represents the loading number of the $[Cu(phen)(cys)(H_2O)]$-

https://doi.org/10.1021/acsomega.2c01858
ACS Omega 2022, 7, 26190−26200

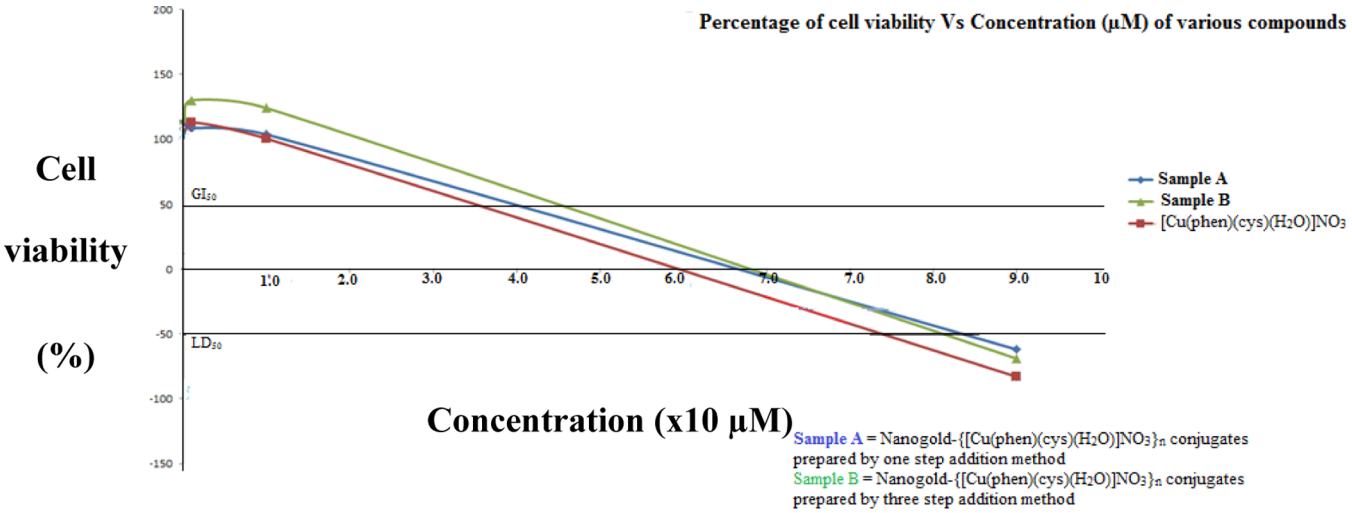

Figure 15. MTS assay of nanogold−{[Cu(phen)(cys)(H_2O)]NO_3}$_n$ conjugates on a breast cancer cell line (MCF7).

Table 2. GI_{50}, TGI, and LD_{50} Values of Nanogold−{[Cu(phen)(cys)(H_2O)]NO_3}$_n$ Conjugate Samples (A and B) and the Free [Cu(Phen)(cys)(H_2O)]NO_3 Complex on the Normal Cell Line (MCF10A)

sample	GI_{50} (μM)	TGI (μM)	LD_{50} (μM)
sample A	nil	nil	nil
sample B	nil	nil	nil
[Cu(Phen)(Cys)(H_2O)]NO_3	7.2	nil	nil

Table 3. GI_{50}, TGI, and LD_{50} Values of Nanogold−{[Cu(phen)(cys)(H_2O)]NO_3}$_n$ Conjugate Samples (A and B) and the Free {Cu(phen)(cys)(H_2O)]NO_3 Complex on the Breast Cancer Cell Line (MCF7)

sample	GI_{50} (μM)	TGI (μM)	LD_{50} (μM)
sample A	3.95	6.63	8.3
sample B	4.48	6.8	8.1
[Cu(Phen)(Cys)(H_2O)]NO_3	3.5	5.94	7.38

NO_3 complex per gold nanoparticle. Nanogold−{[Cu(phen)-(cys)(H_2O)]NO_3}$_n$ conjugate particles generated in this study had a spherical shape with a size distribution of a few hundred nanometers. Hence, the exact concentration of the conjugate on the basis of gold particles could not be determined. Although the conjugate concentration was overestimated, the data presented in Figures 14 and 15 are comparable because the sample concentration and the serial dilution used in both the cell lines (MCF10A and MCF7) were the same.

CONCLUSIONS

The novel nanogold−{[(Cu)(phen)(cys)(H_2O)]NO_3}$_n$ conjugate was successfully synthesized via (i) the direct reaction between the nanogold and [(Cu)(phen)(cys)(H_2O)]NO_3 complex in the aqueous solution, and (ii) the sequential addition of the nanogold solution with L-cysteine, copper nitrate, and lastly, 1,10-phenanthroline. The nanogold was bonded to the copper complex by the thiol group of L-cysteine. The MTS assay study showed that the nanogold−copper complex conjugates were not cytotoxic against the normal cells (MCF10A) in the tested molar concentrations, but their unbound analog, the free [(Cu)(phen)(cys)(H_2O)]NO_3 complex, caused significant toxicity. It was also observed that, in the tested concentration range, the nanogold−copper complex conjugates caused selective inhibition and breast cancer cell (MCF7) death.

AUTHOR INFORMATION

Corresponding Author

Ing Hong Ooi − *Department of Pharmaceutical Chemistry, School of Pharmacy, International Medical University, Kuala Lumpur 57000, Malaysia;* orcid.org/0000-0002-8270-126X; Email: inghong_ooi@imu.edu.my

Authors

Ahmad Junaid − *Department of Pharmaceutical Chemistry, School of Pharmacy, International Medical University, Kuala Lumpur 57000, Malaysia;* Present Address: Department of Medicinal Chemistry and Molecular Pharmacology, Purdue University, 575 Stadium Mall Drive, West Lafayette, Indiana 47907, United States

Chew Hee Ng − *Department of Pharmaceutical Chemistry, School of Pharmacy, International Medical University, Kuala Lumpur 57000, Malaysia*

Complete contact information is available at: https://pubs.acs.org/10.1021/acsomega.2c01858

Notes

The authors declare no competing financial interest.

ACKNOWLEDGMENTS

The authors wish to thank International Medical University for the financial support and Ng Pei Ying for her assistance in conducting the MTS assay.

REFERENCES

(1) Mertz, W. The Essential Trace Elements. *Science* **1981**, *213*, 1332−1338.
(2) Frieden, E. New Perspectives on the Essential Trace Elements. *J. Chem. Educ.* **1985**, *62*, 917−923.
(3) Kubova, K. Biological Role of Copper as an Essential Trace Element in the Human Organism. *Ceska Slov. Farm.* **2018**, *67*, 143−153.
(4) Pan, Y.-J.; Loo, G. Effect of Copper Deficiency on Oxidative DNA Damage in Jurkat T-lymphocytes. *Free Radical Biol. Med.* **2000**, *28*, 824−830.

(5) Uriu-Adams, J. Y.; Keen, C. L. Copper, Oxidative Stress, and Human Health. *Mol. Aspects Med.* **2005**, *26*, 268−298.
(6) Krasnovskaya, O.; Naumov, A.; Guk, D.; Gorelkin, P.; Erofeev, A.; Beloglazkina, E.; Majouga, A. Copper Coordination Compounds as Biologically Active Agents. *Int. J. Mol. Sci.* **2020**, *21*, 3965.
(7) Santini, C.; Pellei, M.; Gandin, V.; Porchia, M.; Tisato, F.; Marzano, C. Advances in Copper Complexes as Anticancer Agents. *Chem. Rev.* **2014**, *114*, 815−862.
(8) Hussain, A.; AlAjmi, M. F.; Rehman, M. T.; Amir, S.; Husain, F. M.; Alsalme, A.; Siddiqui, M. A.; AlKhedhairy, A. A.; Khan, R. A. Copper(II) Complexes as Potential Anticancer and Nonsteroidal Anti-inflammatory Agents: In Vitro and in Vivo Studies. *Sci. Rep.* **2019**, *9*, 5237.
(9) Northcote-Smith, J.; Johnson, A.; Singh, K.; Ortu, F.; Suntharalingam, K. Breast Cancer Stem Cell Active Copper(II) Complexes with Naphthol Schiff Base and Polypyridyl Ligands. *Inorganics* **2021**, *9*, 5.
(10) Deegan, C.; McCann, M.; Devereux, M.; Coyle, B.; Egan, D. A. In Vitro Cancer Chemotherapeutic Activity of 1,10-Phenanthroline (phen), $[Ag_2(phen)_3(mal)]\cdot 2H_2O$, $[Cu(phen)_2(mal)]\cdot 2H_2O$ and $[Mn(phen)_2(mal)]\cdot 2H_2O$ ($malH_2$ = malonic acid) using Human Cancer Cells. *Cancer Lett.* **2007**, *247*, 224−233.
(11) Mo, X.; Chen, Z.; Chu, B.; Liu, D.; Liang, Y.; Liang, F. Structure and Anticancer Activities of Four Cu(II) Complexes Bearing Tropolone. *Metallomics* **2019**, *11*, 1952−1964.
(12) Rostas, A. M.; Badea, M.; Ruta, L. L.; Farcasanu, I. C.; Maxim, C.; Chifiriuc, M. C.; Popa, M.; Luca, M.; Celan Korosin, N.; Cerc Korosec, R.; Bacalum, M.; Raileanu, M.; Olar, R. Copper(II) Complexes With Mixed Heterocycle Ligands as Promising Antibacterial and Antitumor Species. *Molecules* **2020**, *25*, 3777.
(13) Harris, L. J. On a Series of Metallo-Cystein Derivatives. 1. *Biochem. J.* **1922**, *16*, 739−746.
(14) Wharton, H. W. The Copper(II) Derivatives of S-(1,2-trans-dichlorovinyl)-L-Cysteine and Related Compounds. Retrospective Theses and Dissertations, Iowa State University, 1960.
(15) Quan, X.; Uddin, R.; Heiskanen, A.; Parmvi, M.; Nilson, K.; Donolato, M.; Hansen, M. F.; Rena, G.; Boisen, A. The Copper Binding Properties of Metformin - QCM-D, XPS and Nanobead Agglomeration. *Chem. Commun.* **2015**, *51*, 17313−17316.
(16) Dokken, K. M.; Parsons, J. G.; McClure, J.; Gardea-Torresdey, J. L. Synthesis and Structural Analysis of Copper(II) Cysteine Complexes. *Inorg. Chim. Acta* **2009**, *362*, 395−401.
(17) Meir, R.; Shamalov, K.; Betzer, O.; Motiei, M.; Horovitz-Fried, M.; Yehuda, R.; Popovtzer, A.; Popovtzer, R.; Cohen, C. J. Nanomedicine for Cancer Immunotherapy: Tracking Cancer-Specific T-Cells In Vivo with Gold Nanoparticles and CT Imaging. *ACS Nano* **2015**, *9*, 6363−6372.
(18) Pokharkar, V.; Bhumkar, D.; Suresh, K.; Shinde, Y.; Gairola, S.; Jadhav, S. S. Gold Nanoparticles as a Potential Carrier for Transmucosal Vaccine Delivery. *J. Biomed. Nanotechnol.* **2011**, *7*, 57−59.
(19) Wang, F.; Wang, Y.-C.; Dou, S.; Xiong, M.-H.; Sun, T.-M.; Wang, J. Doxorubicin-Tethered Responsive Gold Nanoparticles Facilitate Intracellular Drug Delivery for Overcoming Multidrug Resistance in Cancer Cells. *ACS Nano* **2011**, *5*, 3679−3692.
(20) Saha, K.; Agasti, S. S.; Kim, C.; Li, X.; Rotello, V. M. Gold Nanoparticles in Chemical and Biological Sensing. *Chem. Rev.* **2012**, *112*, 2739−2779.
(21) Seyyedi, N.; Farjadian, F.; Farhadi, A.; Rafiei Dehbidi, G.; Ranjbaran, R.; Zare, F.; Ali Okhovat, M.; Nikouyan, N.; Behzad-Behbahani, A. High Yield Gold Nanoparticle-Based DNA Isolation Method for Human Papillomaviruses Genotypes from Cervical Cancer Tissue Samples. *IET Nanobiotechnol.* **2020**, *14*, 555−562.
(22) Frens, G. Controlled Nucleation for the Regulation of the Particle Size in Monodisperse Gold Suspensions. *Nat. Phys. Sci.* **1973**, *241*, 20−22.
(23) Netti, P. A.; Baxter, L. T.; Boucher, Y.; Skalak, R.; Jain, R. K. Time-Dependent Behavior of Interstitial Fluid Pressure in Solid Tumors: Implications for Drug Delivery. *Cancer Res.* **1995**, *55*, 5451−5458.
(24) Rakesh, K. J. The Next Frontier of Molecular Medicine: Delivery of Therapeutics. *Nat. Med.* **1998**, *4*, 655−657.
(25) Singh, P.; Pandit, S.; Mokkapati, V. R. S. S.; Garg, A.; Ravikumar, V.; Mijakovic, I. Gold Nanoparticles in Diagnostics and Therapeutics for Human Cancer. *Int. J. Mol. Sci.* **2018**, *19*, 1979.
(26) Javier, D. J.; Nitin, N.; Levy, M.; Ellington, A.; Richards-Kortum, R. Aptamer-Targeted Gold Nanoparticles as Molecular-Specific Contrast Agents for Reflectance Imaging. *Bioconjugate Chem.* **2008**, *19*, 1309−1312.
(27) Taton, T. A. Preparation of Gold Nanoparticle-DNA Conjugates. In *Current Protocols in Nucleic Acid Chemistry*; Beaucage, S. L., Ed., 2002. Chapter 12, Unit 12.2.
(28) Kalmodia, S.; Vandhana, S.; Tejaswini Rama, B. R.; Jayashree, B.; Sreenivasan Seethalakshmi, T.; Umashankar, V.; Yang, W.; Barrow, C. J.; Krishnakumar, S.; Elchuri, S. V. Bio-Conjugation of Antioxidant Peptide on Surface-Modified Gold Nanoparticles: A Novel Approach to Enhance the Radical Scavenging Property in Cancer Cell. *Cancer Nanotechnol.* **2016**, *7*, 1.
(29) West, J. L.; Drezek, R.; Sershen, S.; Halas, N. J. Optically Absorbing Nanoparticles for Enhanced Tissue Repair. U.S. Patent 6,685,730 B2.
(30) Connor, E. E.; Mwamuka, J.; Gole, A.; Murphy, C. J.; Wyatt, M. D. Gold Nanoparticles are Taken Up by Human Cells but Do Not Cause Acute Cytotoxicity. *Small* **2005**, *1*, 325−327.
(31) Paciotti, G. F.; Myer, L.; Weinreich, D.; Goia, D.; Pavel, N.; McLaughlin, R. E.; Tamarkin, L. Colloidal Gold: A Novel Nanoparticle Vector for Tumor Directed Drug Delivery. *Drug Delivery* **2004**, *11*, 169−183.
(32) Bromma, K.; Chithrani, D. B. Advances in Gold Nanoparticle-Based Combined Cancer Therapy. *Nanomaterials* **2020**, *10*, 1671−1695.
(33) Rao, R.; Patra, A. K.; Chetana, P. R. Structure, DNA Binding and Oxidative Cleavage Activity of Ternary (L-Leucine/Isoleucine) Copper(II) Complexes of Heterocyclic Bases. *Polyhedron* **2008**, *27*, 1343−1352.
(34) Zhao, P.; Li, N.; Astruc, D. State of the Art in Gold Nanoparticle Synthesis. *Coord. Chem. Rev.* **2013**, *257*, 638−665.
(35) Ferreira, M. F.; Mousavi, B.; Ferreira, P. M.; Martins, C. I. O.; Helm, L.; Martins, J. A.; Geraldes, C. F. G. C. Gold Nanoparticles Functionalized with Stable, Fast Water Exchange Gd^{3+} Chelates as High Relaxivity Contrast Agents for MRI. *Dalton Trans.* **2012**, *41*, 5472−5475.
(36) Ghosh, P.; Han, G.; De, M.; Kim, C.; Rotello, V. Gold Nanoparticles in Delivery Applications. *Adv. Drug Delivery Rev.* **2008**, *60*, 1307−1315.
(37) Mocanu, A.; Cernica, I.; Tomoaia, G.; Bobos, L.-D.; Horovitz, O.; Tomoaia-Cotisel, M. Self-Assembly Characteristics of Gold Nanoparticles in the Presence of Cysteine. *Colloids Surf., A* **2009**, *338*, 93−101.
(38) Seng, H.-L.; Wang, W.-S.; Kong, S.-M.; Alan Ong, H.-K.; Win, Y.-F.; Raja Abd. Rahman, R. N. Z.; Chikira, M.; Leong, W.-K.; Ahmad, M.; Khoo, A. S.-B.; Ng, C.-H. Biological and Cytoselective Anticancer Properties of Copper(II)-Polypyridyl Complexes Modulated by Auxiliary Methylated Glycine Ligand. *BioMetals* **2012**, *25*, 1061−1081.
(39) Ng, C.-H.; Wang, W.-S.; Chong, K.-V.; Win, Y.-F.; Neo, K.-E.; Lee, H.-B.; San, S.-L.; Raja Abd. Rahman, R. N. Z.; Leong, W. K. Ternary Copper(II)-Polypyridyl Enantiomers: Aldol-Type Condensation, Characterisation, DNA-Binding Recognition, BSA-Binding and Anticancer Property. *Dalton Trans.* **2013**, *42*, 10233−10243.
(40) Ng, C. H.; Chan, C. W.; Lai, J. W.; Ooi, I. H.; Chong, K. V.; Maah, M. J.; Seng, H. L. Enantiomeric Pair of Copper(II) Polypyridyl-Alanine Complexes: Effect of Chirality on Their Interaction with Biomolecules. *J. Inorg. Biochem.* **2016**, *160*, 1−11.
(41) Schilt, A. A.; Taylor, R. C. Infra-Red Spectra of 1,10-Phenanthroline Metal Complexes in the Rock Salt Region below 2000 cm^{-1}. *J. Inorg. Nucl. Chem.* **1959**, *9*, 211−221.

https://doi.org/10.1021/acsomega.2c01858
ACS Omega 2022, 7, 26190−26200